TM-Radiation From an Obliquely Flanged Parallel-Plate Waveguide

Jae Yong Kwon, *Member, IEEE*, Jae Wook Lee, *Associate Member, IEEE*, and Hyo Joon Eom, *Senior Member, IEEE*

***Abstract*—Electromagnetic TM wave radiation from an obliquely flanged parallel-plate waveguide is studied. The Fourier-transform/series and Green's formula is used to represent the scattered wave and the simultaneous equations for the modal coefficients are formulated. Residue calculus is utilized to obtain a fast-convergent series solution. Numerical evaluation shows the behaviors of transmission, reflection, and radiation in terms of junction geometry and operating frequency.**

***Index Terms*—Fourier transform, mode matching, residue arithmetic, waveguide bends.**

I. Introduction

Electromagnetic radiation from a flanged parallel-plate waveguide is an important subject due to its flush-mounted antenna and waveguide junction applications. Radiation from a right-angled, infinitely flanged parallel-plate waveguide has been extensively studied and its behaviors are well understood [1] and [2]. Radiation from an obliquely flanged parallel-plate waveguide is of some theoretical interest, but its radiation study is relatively very little [3], [4]. Scattering from an infinite number of inclined strips [5] and inclined parallel-plate waveguides [6] have been also studied with mode-matching technique. In this paper, we intend to study transverse-magnetic-to-wave-propagation (TM) wave radiation from an obliquely flanged parallel-plate waveguide, using the Fourier transform and series representations. In Sections II and III, we will present convergent series solutions for reflection, transmission, and radiation, and illustrate their numerical behaviors.

II. TM Field Representations

Consider a TM wave radiating from an obliquely flanged parallel-plate waveguide into a conducting plane as shown in Fig. 1. When a conducting plane is removed, the scattering geometry becomes a half-space radiation problem. The wavenumber is k ($= 2\pi/\lambda$, λ: wavelength) and an $e^{-i\omega t}$ time–harmonic convention is suppressed.

In region (I), the total incident and reflected H fields are

$$H_y^i(x,z) = \cos(a_p x) e^{ik_p z} \tag{1}$$

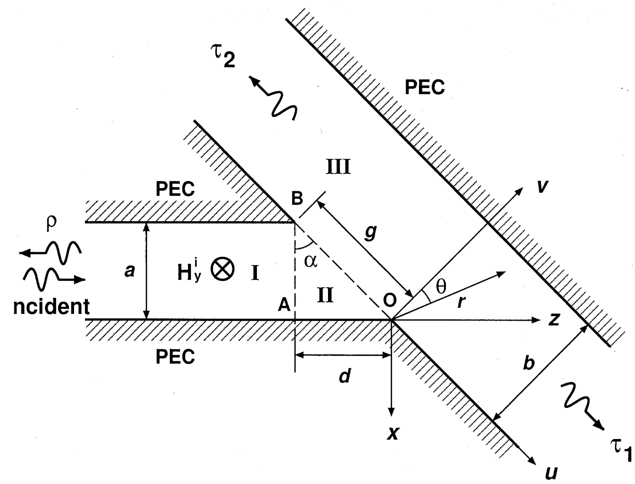

Fig. 1. Obliquely flanged parallel-plate waveguide.

$$H_y^r(x,z) = \sum_{m=0}^{\infty} B_m \cos(a_m x) e^{-ik_m z} \tag{2}$$

where $a_p = p\pi/a$ and $k_p = \sqrt{k^2 - a_p^2}$.

In region (III), the H field is

$$H_y^{III}(u,v) = \frac{1}{2\pi}\int_{-\infty}^{\infty} \left[\tilde{H}_+(\zeta)e^{i\kappa v} + \tilde{H}_-(\zeta)e^{-i\kappa v}\right] e^{-i\zeta u} d\zeta \tag{3}$$

where $\kappa = \sqrt{k^2 - \zeta^2}$.

Let us relate the fields in regions I and III, by applying the second Green's formula [6], [7]

$$\oint_c \left(H_y \frac{\partial G}{\partial \nu} - G \frac{\partial H_y}{\partial \nu} \right) dl = 0 \tag{4}$$

where the symbol c denotes the contour OAB (Fig. 1). The auxiliary function, which satisfies the Helmholtz equation in region I, is chosen to be

$$G_q^{\pm} = \cos(a_q x) e^{\pm i k_q z}, \quad q = 0, 1, 2, \ldots. \tag{5}$$

Note that G_q^+ and G_q^- are linearly independent of each other [5]. The fields on the line OB are written in a Fourier series on the interval $(-g, 0)$

$$H_y\big|_{OB} = \sum_{n=-\infty}^{\infty} C_n e^{i(2\pi n/g)u} \tag{6}$$

$$\frac{\partial H_y}{\partial v}\bigg|_{OB} = \sum_{n=-\infty}^{\infty} D_n e^{i(2\pi n/g)u} \tag{7}$$

where C_n and D_n are unknown coefficients.

Manuscript received January 18, 2001; revised May 30, 2001.

J. Y. Kwon is with the Digital Media Research Laboratory, LG Electronics, Inc., Seoul, 137–724, Korea.

J. W. Lee is with the Advanced Radio Technology Department, Electronics and Telecommunications Research Institute, Daejon 305-701, Korea.

H. J. Eom is with the Department of Electrical Engineering and Computer Science, Korea Advanced Institute of Science and Technology, Daejon 305-701, Korea (e-mail: hjeom@ee.kaist.ac.kr).

Digital Object Identifier 10.1109/TAP.2002.803964

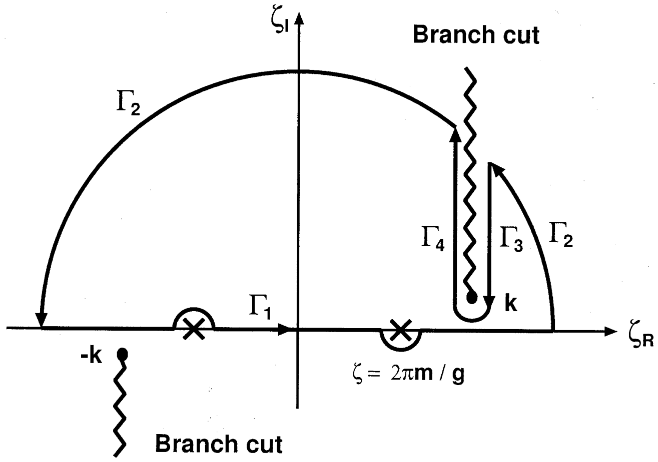

Fig. 2. Closed path for contour integration in ζ plane.

Substituting G_q^+ in (5) and the fields in (6)-(7) into (4) gives

$$\sum_{m=0}^{\infty} B_m i a k_q \varepsilon_q \delta_{mq} = \sum_{n=-\infty}^{\infty} \left[C_n \left(a_q g_q \sin\alpha + k_q \cos\alpha \chi_n^+\right) + D_n i \chi_n^+\right] \Lambda_q\left(\chi_n^+\right). \quad (8)$$

Similarly substituting G_q^-, in (5) and the fields in (6)-(7) into (4) gives

$$-iak_q\varepsilon_q\delta_{pq} = \sum_{n=-\infty}^{\infty} \left[C_n \left(a_q g_q \sin\alpha - k_q \cos\alpha \chi_n^-\right) + D_n i \chi_n^-\right] \Lambda_q\left(\chi_n^-\right) \quad (9)$$

where $g_q = q\pi/g$, $\Lambda_q(\zeta) = (1-(-1)^q e^{-ig\zeta})/(g_q^2-\zeta^2)$, $\chi_n^\pm = (2\pi n/g) \pm k_q \sin\alpha$, $q = 0, 1, 2, \ldots$, and δ_{pq} is the Kronecker delta.

The E_u continuity at $v = b$ yields

$$\tilde{H}_-(\zeta) = \tilde{H}_+(\zeta)e^{i2\kappa b}. \quad (10)$$

The E_u continuity at $v = 0$ between regions II and III is

$$\frac{1}{\omega\epsilon}\frac{1}{2\pi}\int_{-\infty}^{\infty}\left[\tilde{H}_+(\zeta) - \tilde{H}_-(\zeta)\right]\kappa e^{-i\zeta u} d\zeta = \begin{cases} \frac{1}{i\omega\epsilon}\sum\limits_{n=-\infty}^{\infty} D_n e^{i(2\pi n/g)u}, & \text{for } -g < u < 0 \\ 0, & \text{otherwise.}\end{cases} \quad (11)$$

Taking the Fourier transform of (11) results in

$$[\tilde{H}_+(\zeta) - \tilde{H}_-(\zeta)]\kappa = -\sum_{n=-\infty}^{\infty} D_n F_n^-(\zeta) \quad (12)$$

where $F_n^\pm(\zeta) = (1 - e^{\pm ig\zeta})/(\zeta + (2\pi n/g))$.

The H_y continuity at $v = 0$ yields

$$\sum_{n=-\infty}^{\infty} C_n e^{i(2\pi n/g)u} = \frac{1}{2\pi}\int_{-\infty}^{\infty}[\tilde{H}_+(\zeta) + \tilde{H}_-(\zeta)]e^{-i\zeta u}d\zeta. \quad (13)$$

Substituting (10) and (12) into (13), multiplying (13) by $e^{-i(2\pi m/g)u}$, and performing integration with respect to u from $-g$ to 0 yields

$$C_m = \sum_{n=-\infty}^{\infty} \frac{D_n}{g} I_{mn} \quad (14)$$

where

$$I_{mn} = \frac{1}{2\pi}\int_{-\infty}^{\infty}\frac{\cot(\kappa b)}{\kappa}F_m^+(\zeta)F_n^-(\zeta)d\zeta. \quad (15)$$

We transform I_{mn} into a rapidly-convergent series by utilizing the residue calculus as

$$I_{mn} = -i\sum_{t=0}^{\infty}\frac{2(1-e^{ig\zeta_t})}{b\zeta_t\varepsilon_t}\frac{\left[\zeta_t^2 + \left(\frac{2\pi}{g}\right)^2 mn\right]}{\left[\zeta_t^2 - \left(\frac{2\pi m}{g}\right)^2\right]\left[\zeta_t^2 - \left(\frac{2\pi n}{g}\right)^2\right]} + g\delta_{mn}\frac{\cot\left(b\sqrt{k^2 - \left(\frac{2\pi n}{g}\right)^2}\right)}{\sqrt{k^2 - \left(\frac{2\pi n}{g}\right)^2}} \quad (16)$$

where $\zeta_t = \sqrt{k^2 - (t\pi/b)^2}$, $\varepsilon_t = \begin{cases} 2, & \text{when } t = 0 \\ 1, & t = 1, 2, 3, \ldots. \end{cases}$

When b goes to ∞ (half space), it is more convenient to transform (15) into a fast-convergent branch-cut integral. Consider a deformed contour path shown in Fig. 2. Performing a contour integration, we transform (15) into a pole contribution at $\zeta = 2\pi m/g$ $(m = n)$ and branch-cut integral along Γ_3 and Γ_4 associated with a branch point $\zeta = k$. The result is shown in (17) at the bottom of the next page. A set of simultaneous (8), (9), and (14) constitutes the final formulation and must be numerically evaluated for the modal coefficients B_m, C_n, and D_n. The scattered fields at $u = \pm\infty$ in region III is then

$$H_y^{III}(\pm\infty, v) = \sum_t K_t^\pm \cos b_t(v-b)e^{\pm i\zeta_t u} \quad (18)$$

where

$$K_t^\pm = -\sum_{n=-\infty}^{\infty} D_n \frac{1 - e^{\pm i\zeta_t g}}{b\zeta_t\varepsilon_t(-1)^t\left(\mp\zeta_t + \frac{2\pi n}{g}\right)} \quad (19)$$

$b_t = (t\pi/b)$, $0 \le t$, t: integer.

The transmission (τ_1, τ_2) and reflection (ρ) coefficients in Fig. 1 are

$$\tau_1 = \frac{b}{a\varepsilon_p k_p}\sum_t \varepsilon_t\zeta_t|K_t^+|^2 \quad (20)$$

$$\tau_2 = \frac{b}{a\varepsilon_p k_p}\sum_t \varepsilon_t\zeta_t|K_t^-|^2 \quad (21)$$

$$\rho = \sum_m \frac{\varepsilon_m k_m}{\varepsilon_p k_p}|B_m|^2 \quad (22)$$

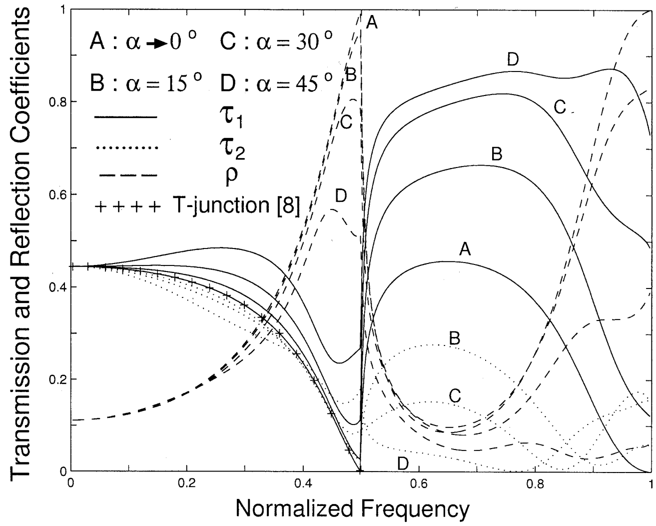

Fig. 3. Behavior of transmission (τ_1, τ_2) and reflection (ρ) coefficients versus the normalized frequency $(ka/2\pi)$ for the oblique parallel-plate waveguide ($a/b = 1, p = 0$).

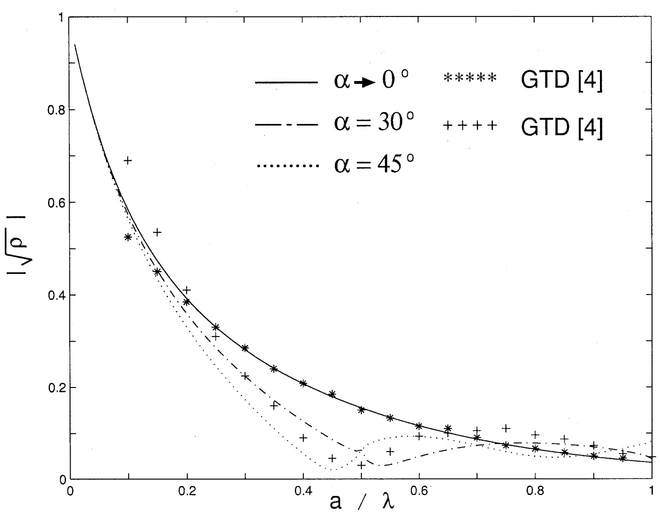

Fig. 4. TEM reflection coefficient magnitude for various α with $b \to \infty$.

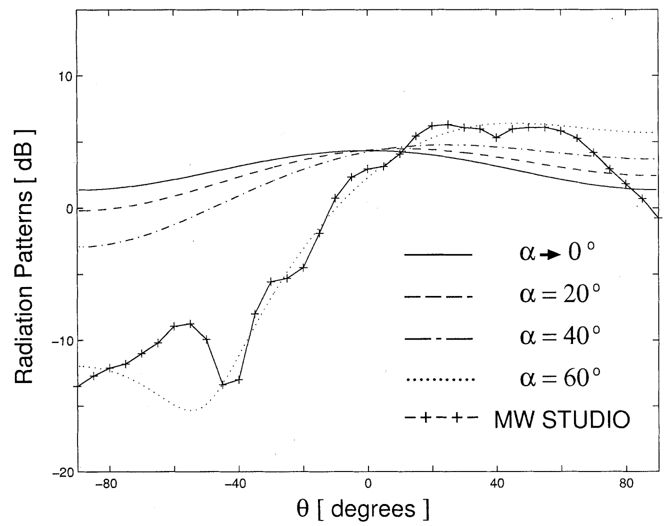

Fig. 5. Behavior of angular radiation pattern ($b \to \infty$).

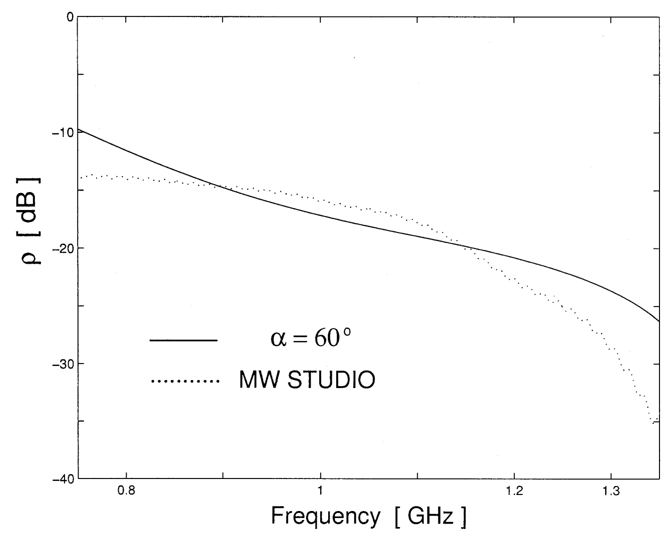

Fig. 6. Reflection coefficient magnitude for $\alpha = 60°$ with $b \to \infty$ ($a = 12$ cm).

where $0 \leq t < (kb/\pi)$, t: integer, $0 \leq m < (ka/\pi)$, m: integer. When b goes to ∞, the far-zone scattered field at distance r from the origin is

$$H_y^{III}(\theta) = \sqrt{\frac{1}{2\pi kr}} e^{i(kr-(\pi/4))}[k\cos\theta \tilde{H}_+(-k\sin\theta)]. \quad (23)$$

III. Numerical Evaluations

In this section, we show the numerical results to illustrate the radiation and scattering properties of obliquely flanged parallel-plate waveguide. Fig. 3 shows the TM wave behavior of transmission (τ_1, τ_2) and reflection (ρ) coefficients versus the normalized frequency (ka/π). The incident field is assumed to be (1) with $p = 0$. We check the numerical accuracy of our approach by confirming the energy conservation ($\tau_1 + \tau_2 + \rho = 1$). The number of the modal coefficients used in (8) and (9) must be large enough to include the propagation plus several higher-evanescent modes for numerical accuracy. In Fig. 3, our computational experience indicates that the rate of series convergence to achieve numerical accuracy is inversely proportional to the taper angle α. When $\alpha \to 0°$, our

$$I_{mn} = -\frac{2i}{\pi}\int_0^\infty \frac{[1-e^{igk(1+iv)}]}{\sqrt{v(v-2i)}} \frac{\left[k^2(1+iv)^2 + \left(\frac{2\pi}{g}\right)^2 mn\right]}{\left[k^2(1+iv)^2 - \left(\frac{2\pi m}{g}\right)^2\right]\left[k^2(1+iv)^2 - \left(\frac{2\pi n}{g}\right)^2\right]} dv + \delta_{mn}\frac{g}{\sqrt{k^2 - \left(\frac{2\pi m}{g}\right)^2}} \quad (17)$$

TABLE I
CONVERGENCE BEHAVIOR OF $|B_m|$ AND POWER CONSERVATION ERROR VERSUS n AND TAPER ANGLE α WITH $a = 0.3\lambda$, $p = 0$, AND $b \to \infty$ $(m = 0, 1, 2, \ldots, 2n)$

	$\alpha \to 0°$						$\alpha = -15°$					
	$\lvert B_0\rvert$	$\lvert B_1\rvert$	$\lvert B_2\rvert$	$\lvert B_3\rvert$	$\lvert B_4\rvert$	error[%]	$\lvert B_0\rvert$	$\lvert B_1\rvert$	$\lvert B_2\rvert$	$\lvert B_3\rvert$	$\lvert B_4\rvert$	error[%]
n=1	0.2832	0.0000	0.1040	-	-	0.00	0.2692	0.1456	0.0666	-	-	0.83
n=2	0.2823	0.0000	0.1055	0.0000	0.0322	0.00	0.2673	0.1470	0.0686	0.0283	0.0183	0.61
n=3	0.2819	0.0000	0.1062	0.0000	0.0326	0.00	0.2664	0.1472	0.0690	0.0287	0.0193	0.51
n=4	0.2817	0.0000	0.1066	0.0000	0.0329	0.00	0.2660	0.1472	0.0691	0.0288	0.0194	0.46
n=5	0.2815	0.0000	0.1069	0.0000	0.0330	0.00	0.2657	0.1471	0.0692	0.0287	0.0194	0.42
n=6	0.2814	0.0000	0.1071	0.0000	0.0331	0.00	0.2655	0.1470	0.0692	0.0286	0.0193	0.40

	$\alpha = -30°$						$\alpha = -45°$					
	$\lvert B_0\rvert$	$\lvert B_1\rvert$	$\lvert B_2\rvert$	$\lvert B_3\rvert$	$\lvert B_4\rvert$	error[%]	$\lvert B_0\rvert$	$\lvert B_1\rvert$	$\lvert B_2\rvert$	$\lvert B_3\rvert$	$\lvert B_4\rvert$	error[%]
n=1	0.2286	0.2196	0.0601	-	-	4.22	0.1727	0.2397	0.0514	-	-	13.73
n=2	0.2247	0.2185	0.0620	0.0292	0.0168	3.19	0.1687	0.2268	0.0490	0.0212	0.0114	10.08
n=3	0.2237	0.2166	0.0612	0.0290	0.0175	2.77	0.1693	0.2176	0.0450	0.0192	0.0105	8.57
n=4	0.2235	0.2151	0.0602	0.0283	0.0170	2.55	0.1707	0.2109	0.0417	0.0172	0.0092	7.74
n=5	0.2237	0.2138	0.0594	0.0276	0.0164	2.44	0.1721	0.2057	0.0390	0.0155	0.0082	7.18
n=6	0.2240	0.2127	0.0586	0.0269	0.0159	2.37	0.1731	0.2013	0.0369	0.0143	0.0074	6.72

transmission coefficient (τ_1) agrees with the E plane T-junction transmission coefficient (τ_2) in [8]. When $\alpha = 20°$, the energy conservation is satisfied to better than 2% error with $m = 10$ and $n = 5$, indicating a fast convergent rate of our series solution. However, when $\alpha = 45°$, the worst case (7% error in energy conservation) occurs with $m = 10$ and $n = 5$. A variation in τ_1 and τ_2 is less sensitive to a change in α for a single-mode frequency region $((ka/2\pi) = 0 \sim 0.5)$ than for a higher-mode region $((ka/2\pi) > 0.5)$. Fig. 4 describes the TEM reflection coefficient as a function of a/λ for three different taper angles $\alpha = 0°$, $30°$, and $45°$ when $b \to \infty$. Our numerical results are seen to be in a good agreement with the geometric theory of diffraction (GTD) solution in [4]. The TM wave angular radiation patterns are shown in Fig. 5 when $b \to \infty$. It illustrates that an increase in the taper angle α tends to shift a maximum radiation angle (θ) toward $90°$. To check the accuracy of our computation, we compare our result of $\alpha = 60°$ with the numerical data of Computer Simulation Technology (CST) MW STUDIO, which is a commercially available numerical computation tool. The numerical data based on the CST MW STUDIO show the TM wave angular radiation patterns (u-v plane cut) of three-dimensional (3-D) oblique aperture (aperture width in the y direction: 5λ, flange width: $4\lambda \times 4\lambda$). It is seen that the numerical data based on the MW STUDIO agree favorably with our theory except for some discrepancies near the endfire direction. The discrepancies may be attributed to the fact that our theory assumes a parallel-plate waveguide (0.4λ) with an infinite flange whereas the MW STUDIO uses a rectangular waveguide $(0.4\lambda \times 5\lambda)$ with a finite-sized $(4\lambda \times 4\lambda)$ flange. In Fig. 6, we compare our theory with the MW STUDIO which evaluates the reflection coefficient of a 3-D oblique aperture (WR-975 rectangular waveguide). In order to compare our theory with the 3-D result, we replace k_m in (1) and (2) with $k_m = \sqrt{k^2 - a_m^2 - (\pi/0.25)^2}$ [9]. The comparison between our theory and the MW STUDIO result reveals a good agreement in a single-mode operating frequency band (0.75–1.12 GHz). Discrepancies between two results become pronounced in a higher frequency regime beyond the TE_{01} cutoff frequency (1.25 GHz). In what follows, we discuss the rate of numerical convergence for our computation in term of the number of modes n and the taper angle α. Table I shows the convergence behavior of $|B_m|$ and power conservation error versus n and the taper angle α. As α increases, the convergence rate for $|B_m|$ slows down and the error in energy conservation becomes pronounced. In order to further investigate the rate of numerical convergence, we plot in Fig. 7 the condition number for the system of simultaneous (9) used in Table I. Note that the condition number increases exponentially as the number of modes n increases linearly. An increase in α results in an increase in the condition number, thus indicating an increase in numerical instability. We also plot the convergence behavior for the tangential field component $H_y|_{OB}$ for different n in Fig. 8. It is seen that slow convergence in the tangential field $H_y|_{OB}$ is observed near the acute wedge $(-0.5 < u/g < 0)$ while fast convergence is achieved at the other end.

IV. CONCLUSION

TM wave radiation from an obliquely flanged parallel-plate guide is investigated using the Fourier transform/series

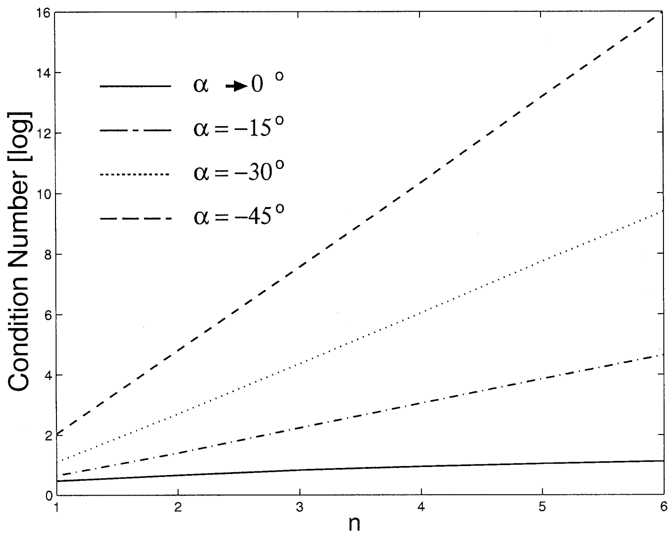

Fig. 7. Condition number of simultaneous (9) versus n with $b \rightarrow \infty$ and $a = 0.3\lambda$.

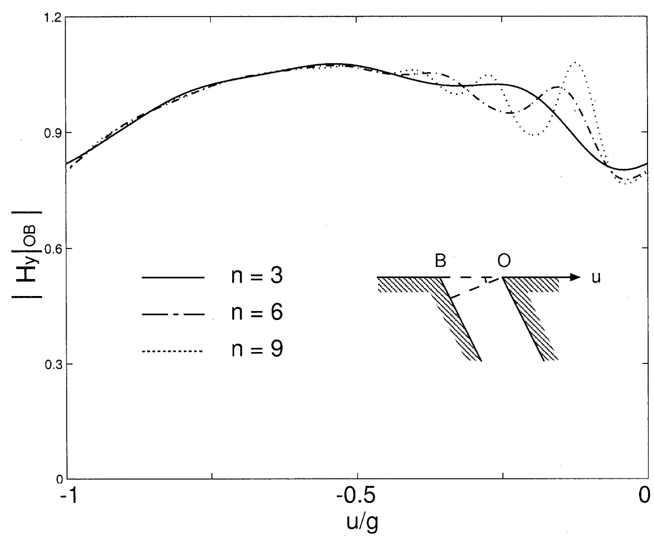

Fig. 8. Magnitude of tangential magnetic field component at the waveguide aperture with $\alpha = -30^\circ$, $b \rightarrow \infty$, and $a = 0.3\lambda$.

technique. Rigorous solutions for radiation and reflection are obtained in numerically efficient forms based on a residue calculus. Numerical computations are performed to illustrate the radiation and reflection behavior of obliquely flanged parallel-plate waveguide. The numerical convergence in our series solution is discussed in terms of the condition number and the error in energy conservation. It is shown that our theory is applicable to the problem of radiation from an obliquely flanged rectangular waveguide.

References

[1] C. H. Kim, H. J. Eom, and T. J. Park, "A series solution for TM-mode radiation from a flanged parallel-plate waveguide," *IEEE Trans. Antennas Propagat.*, vol. 41, pp. 1469–1471, Oct. 1993.

[2] T. J. Park and H. J. Eom, "Analytic solution for TE-mode radiation from a flanged parallel-plate waveguide," *Proc. Inst. Elect. Eng. H*, vol. 140, no. 5, pp. 387–389, Oct. 1993.

[3] Y. N. Vasil'yev and T. A. Kolosova, "Radiation from a tapered open end of a waveguide with an infinite flange," *Radio Eng. Electron. Phys.*, vol. 22, no. 1, pp. 23–30, Jan. 1977.

[4] R. C. Rudduck and L. L. Tsai, "Aperture reflection coefficient of TEM and TE_{01} mode parallel-plate waveguides," *IEEE Trans. Antennas Propagat.*, vol. 16, pp. 83–89, Jan. 1968.

[5] E. E. Kriezis and D. P. Chrissoulidis, "EM-wave scattering by an inclined strip grating," *IEEE Trans. Antennas Propagat.*, vol. 41, pp. 1473–1480, Nov. 1993.

[6] E. A. N. Whitehead, "The theory of parallel-plate media for microwave lenses," *Proc. Inst. Elect. Eng. Lond.*, pt. III, vol. 98, pp. 133–140, Jan. 1951.

[7] M. Born and E. Wolf, *Principles of Optics*. New York: Pergamon, 1975, p. 376.

[8] K. H. Park, H. J. Eom, and Y. Yamaguchi, "An analytic series solution for E-plane T-junction in parallel-plate waveguide," *IEEE Trans. Microwave Theory Tech.*, vol. 42, pp. 356–358, Feb. 1994.

[9] J. W. Lee, H. J. Eom, and J. H. Lee, "TM-wave radiation from flanged parallel plate into dielectric slab," *Proc. Inst. Elect. Eng. -Microwave Antennas Propagat.*, vol. 143, pp. 207–210, June 1996.

Jae Yong Kwon (S'97–M'02) was born in Daegu, Korea, in 1972. He received the B.S. degree in electronics from Kyungpook National University, Daegu, Korea, and the M.S. degree and Ph.D. degrees in electrical engineering from the Korea Advanced Institute of Science and Technology (KAIST), Daejon, Korea, in 1995, 1998, and 2000, respectively.

Since 2002, he has been a Senior Research Engineer with the Digital Media Research Laboratory, LG Electronics, Inc., Seoul, Korea. His research interests include antenna design and wave scattering.

Jae Wook Lee (S'96–A'98) was born in Pohang, Korea, in 1970. He received the B.S. degree in electronic engineering from the Hanyang University, Seoul, Korea, and the M.S. and Ph.D. degrees in electrical engineering from the Korea Advanced Institute of Science and Technology (KAIST) at Daejon, Korea, with an emphasis in electromagnetics, in 1992, 1994, and 1998, respectively.

Since 1998, he has been a Senior Member in the Advanced Radio Technology Department, Radio and Broadcasting Research Laboratory, Electronics and Telecommunications Research Institute, Daejon.

His research interests include computational electromagnetics, antenna design, and high-power amplifier design.

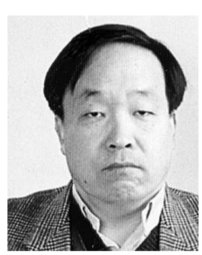

Hyo Joon Eom (S'78–M'82–SM'99) received the B.S. degree in electronic engineering from the Seoul National University, Seoul, Korea, and the M.S. and Ph.D. degrees in electrical engineering from the University of Kansas, Lawrence, in 1973, 1977, and 1982, respectively.

From 1981 to 1984, he was a Research Associate in the Remote Sensing Laboratory, University of Kansas. From 1984 to 1989, he was on the faculty of the Department of Electrical Engineering and Computer Science, University of Illinois, Chicago. In 1989, he joined the Department of Electrical Engineering, KAIST, Daejon, Korea, where he is currently a Professor. His research interests include wave scattering and electromagnetic wave theory.